ELSEVIER

Chemical Engineering Journal 119 (2006) 1–9

Chemical Engineering Journal

www.elsevier.com/locate/cej

Influence of sound wave characteristics on fluidization behaviors of ultrafine particles

Qingjie Guo [a,*], Huie Liu [b], Wenzhong Shen [b], Xianghong Yan [c], Rugao Jia [c]

[a] College of Chemical Engineering, Qingdao University of Science and Technology, Qingdao 266042, Shandong Province, PR China
[b] State Key Laboratory of Heavy Oil Processing, College of Chemistry and Chemical Engineering, China University of Petroleum, Dongying 257061, Shandong Province, PR China
[c] College of Physical Science and Technology, China University of Petroleum, Dongying 257061, Shandong Province, PR China

Received 27 August 2005; received in revised form 16 January 2006; accepted 21 February 2006

Abstract

The fluidization behaviors of ultrafine particles were investigated in an acoustic fluidized bed with one type of micron particles and two types of nanoparticles. With the assistance of sound wave having low sound frequency and high sound pressure level, the micron and nanoparticles can be fluidized smoothly with fluidization behaviors similar to those of Geldart Group A particles. It has been found that increasing sound frequency leads to a reduction in minimum fluidization velocity, and then to an increase in minimum fluidization velocity. At the same sound frequency, the fluidization quality of nanoparticles improves significantly with increasing sound pressure level (100–103.4 dB). In addition, a thorough investigation indicates that sound wave configuration have an influence on fluidization process of ultarfine particles. Experiments show that both Sine wave and Triangle wave can enhance fluidization quality of ultarfine particles.

Keywords: Micron particle; Nanoparticle; Sound frequency; Sound pressure level; Sound wave configuration; Fluidization

1. Introduction

Ultrafine particles are widely used in biomaterials, cosmetics, foods, catalysts, and plastics, due to their extremely small size and much surface area per unit mass. Nevertheless, ultrafine particles are classified as Geldart group C, which is difficult to fluidize owing to strong interparticle forces including van den Waals adhesion forces, electrostatic attractive forces, liquid bridges, hydrogen bonds, and form-closed bonds. It is of importance to develop processing technologies, which can handle effectively large qualities of nanoparticles.

Previous literature [1–4] has reported that fluidization technology is a preferable technique to disperse ultrafine particles in above widespread applications. It has demonstrated that sound wave excites the fluidized bed to break up the large agglomerates yield by cohesive force, therefore achieving a stabilized fluidization. Chirone et al. [5,6] reported bubble-free fluidization at 120 Hz and sound pressure level from 100 to 150 dB by using catalyst, ash and talc micron particles. An acoustic fluidized bed with 40 μm coal fly ash as bed material was employed by Levy et al. [7], who found that increasing sound pressure levels result in a decrease in bed expansion and an increase in bubble frequency. In the subsequent papers, Herrera and Levy [8,9] revealed acoustic standing wave existing throughout the bed, utilizing one-dimensional quasi fluid with constant speed of sound to calculate the sound pressure level data. With respect to acoustic fluidization of nanoparticles, Zhu et al. [10] employed hydrophobic fumed silica nanoparticles (a primary particle size of 12 nm) to observe that there was a significant reduction in minimum fluidization velocity in the presence of sound, and elutriation of nanoparticle agglomerates was much decreased. However, very few experimental findings are available on fluidization behaviors of various nanoparticles using different forms of sound wave, which deserves a systematic research of various nanoparticles and micron particles.

The major objective of this study is to examine the influence of sound frequency and sound pressure level on fluidization behaviors of a variety of micron and nanoparticles. Experimental results concentrate on bed pressure drop, mini-

* Corresponding author. Tel.: +86 546 8396753; fax: +86 546 8391971.
E-mail addresses: Qjguo@mail.hdpu.edu.cn, qj_guo@yahoo.com (Q. Guo).

1385-8947/$ – see front matter © 2006 Elsevier B.V. All rights reserved.
doi:10.1016/j.cej.2006.02.012

Nomenclature

C	sound speed (m/s)
d_p	primary particle size (nm)
f	sound frequency (Hz)
$f(t)$	sound wave function generated by a signal generator
I	acoustic energy density (Pa)
k	wave number
l	a distance of in the medium (m)
P_i	incident wave pressure (Pa)
P_r	reflected wave pressure (Pa)
P_{ia}	amplitude of incident acoustic wave (Pa)
P_{ra}	reflected amplitude of incident acoustic wave (Pa)
$P(x, t)$	total pressure (Pa)
r_p	reflected coefficient
SPL, SPL_0	SPL_0 is the initial sound pressure level and SPL is the local sound pressure level (dB)
t	time (s)
U	voltage generated from a signal generator (mV)
u_{mf}	minimum fluidization velocity (cm/s)
x	distance from the distributor (m)

Greek letters

α	attenuation factor
ρ	particle packed density (kg/m^3)
ω	angular frequency, $\omega = 2\pi f$
φ	fixed phase angle
λ	wave length, $\lambda = c/f$

mum fluidization velocity. In particular, this article presents a detailed investigation regarding fluidization behaviors of micon and nanoparticles with agitation of various forms of sound wave.

2. Experimental

A schematic diagram of the sound agitation fluidized bed is presented in Fig. 1. The fluidized bed is made of glass with a height of 1.6 m and an inner diameter of 0.056 m, using a porous steel plate as the gas distributor. A manometer is installed at 0.03 m above the gas distributor to measure the pressure drop across the bed. The fluidization gas, air, is supplied by a compressor, whose flow rate is measured using four rotameters with various ranges. Table 1 lists the physical properties of the fluidization particles.

Table 1
Physical property of ultrafine particles

Material	d_p (nm)	ρ_p	Type of particles
Cornstarch particle	1.069×10^4	444	Geldart C
SiO_2	500	158	Geldart C
TiO_2	500	178	Geldart C

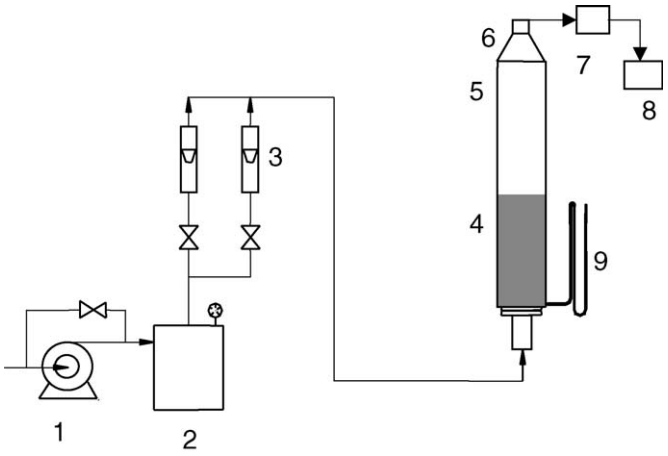

Fig. 1. Schematic diagram of experimental apparatus: 1, compressor; 2, surge tank and desiccator; 3, rotameter; 4, coil; 5, fluidized bed; 6, loudspeaker; 7, sound amplifier; 8, signal generator; 9, manometer.

As illustrated in Fig. 1, the sound source consists of a WY 1603 signal generator, a sound amplifier, and a loudspeaker. WY 1603 signal generator can generate electric pulses with various waveforms including Sine wave, Triangle wave, Square wave, Rampup wave, $\sin(x)/x$, and so on, whose frequency varies in the range from 0.001 to 3 MHz. A 160-mm loudspeaker is fixed at the top of the fluidized bed. The sound level meter was an AZ 8925, with 130 dB maximum pressure value and 0.1 dB precision. Experiments were performed at ambient temperature and atmospheric pressure conditions.

The fluidization behaviors are recorded by a digital camcorder (Sony, DCR-Pc1000E), and then analyzed by a PC computer using a SthVcd software.

3. Results and discussion

3.1. Effect of sound frequency on fluidization behaviors of 500 nm TiO_2

For 500 nm TiO_2 particles, different curves of bed pressure drop versus superficial gas velocity with and without sound excitation are delineated in Fig. 2. An aeration process of 500 nm TiO_2 in the bed consists of three phases: slugging phase, channeling phase, and fluidization phase. As superficial gas velocity is increased from 0.23 to 1.74 cm/s, 500 nm TO_2 particles ascend as a plug characterized by high value of pressure drop owing to wall stress. After bed collapsing, the bed pressure drop reduces greatly resulting from stochastic channels. At a superficial gas velocity of 2.20 cm/s, stable channels takes place in the static bed having a low pressure drop. Observations show that channeling and cracking are accompanied by very unstable the fluidization behaviors of bed. As the superficial gas velocity rises beyond 13.47 cm/s, increased pressure drop reaches a plateau region, suggesting that the bed arrived at a fully fluidization process.

Fig. 2b illustrates that the fluidization process of 500 nm TiO_2 particles is also subject to three phases: slugging phase, channeling phase, and fluidization phase. As expected, 500 nm TiO_2 nanoparticles form a plug causing high values of bed

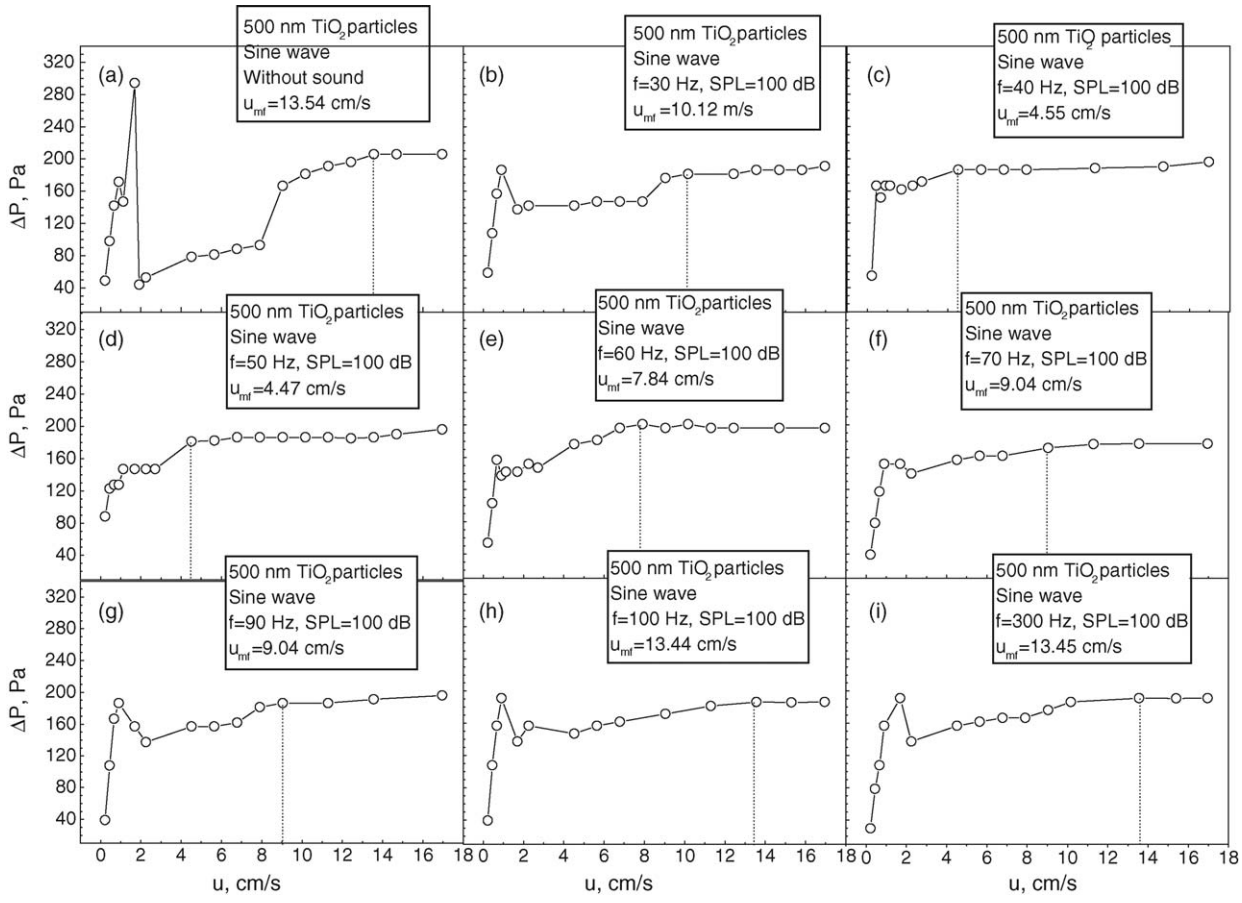

Fig. 2. Effect of sound frequency on the minimum fluidization velocity using 500 nm TiO_2 particles.

pressure drop owing to wall stress at a superficial gas velocity of 0.904 cm/s. At superficial gas velocity exceeding 1.70 cm/s, obvious channels appear in the bed corresponding to low bed pressure drop. The bed fluidized smoothly as superficial gas velocity is greater than 10.12 cm/s. With sound excitation, the disruption of large agglomerate clusters depends on a combine action between hydrodynamic energy and acoustic prompting energy. A low sound frequency leads to a relative low sound energy due to the fact that the sound energy is proportional to the square of sound frequency. Moreover, the hydrodynamic energy has a small value at a low superficial gas velocity. Consequently, the slugging and channeling occur in the bed at low gas velocity. Whereas, the bed can be fully fluidized at high superficial gas velocity ($u > 10.01$ cm/s) because the widespread disruption of large agglomerate clusters takes place result from the increasing combine energy of hydrodynamic energy and acoustic prompting energy.

With respect to fluidization phase, it can be seen that the bed consists of three layers: the upper layer consisting of a small fraction of particle agglomerate in fluidized bed, middle layer forming small agglomerates being in fluidized bed, the bottom layer forming large agglomerates which remains in packed bed. Fluidization behaviors similar to Geldart A particles can be observed at upper layer of the bed owing to the sound energy disrupting the particle agglomerates. However, the large particle agglomerates are still deposited at the bottom of the bed where some regions are kept at fixed bed conditions.

When an acoustic wave propagates through a medium, acoustic wave intensity reduces owing to the attenuation effect of the medium. The attenuation variation can be described by the following relationship [11]:

$$\mathrm{SPL} \propto \mathrm{SPL}_0 l^{-2} \mathrm{e}^{-2\alpha l} \quad (1)$$

where SPL_0 is the initial sound pressure level, SPL the local sound pressure level when acoustic wave propagates in the medium for a distance of l, and α is the attenuation coefficient. Eq. (1) demonstrates the exponential decrease of the sound pressure level with increasing length. The quantification distribution of SPL along the bed height deserves further effort.

The sound energy attenuates greatly as the sound wave propagates through the upper fluidized region and fixed bed region at the bottom region. At this case, the insufficient sound energy cannot break up the particle agglomerates at bottom layer of the fluidized bed and the airflow was not large enough to fluidize such large particle agglomerates. With superficial gas velocity exceeding 10.12 cm/s, the gas hydrodynamic force suspends large agglomerates which reduced the fixed bed region having relative high voidage; therefore, sound wave consumes less energy during attenuation. Accordingly, the sound energy breaks up most of large agglomerates at bed bottom region. By sound

activation, large agglomerate clusters break up due to the combine effects of hydrodynamic forces and acoustic energy, causing fluidization of nanometer particle agglomerate.

At f equals 40 or 50 Hz, it can be observed from Fig. 2c and d, that the minimum fluidization velocity reduces dramatically. Apparently, the fluidization behaviors of nanoparticle are similar to those of Geldart group A. Fig. 2e and f shows that the increasing sound frequency yields a substantial increase in minimum fluidization velocity. On the basis of Stokes–Kirchhoff's formula [12], sound absorption coefficient is proportional to the square of sound frequency as sound propagates through the fluidized bed. It follows that an increase in sound frequency causes increasing sound coefficient, most of sound wave energy is absorbed by the upper part of fluidized bed and decreasing sound energy reaching bottom region fails to disrupt to large agglomerates at the bottom region of the bed.

At f = 90 and 100 Hz, Fig. 2g and h, the bed undergoes the obvious plugging, implying that there exists a peak in the bed pressure drop curve. The possible reason is that the period is short in comparison with the time require for pulsating drag forces acting on inertial force to produce significant detachment of subclusters from clusters. It is anticipated that the minimum fluidization velocity grows further with increasing sound frequencies.

As shown in Fig. 2i, the minimum fluidization velocity rises to 13.45 cm/s at sound frequencies of 300 Hz. In summary, 500 nm TiO_2 particles can reach homogeneous fluidization over a wide sound frequency range from 40 to 70 Hz.

3.2. *Effect of sound frequency on fluidization behaviors of 500 nm SiO_2*

Fig. 3a indicates that the aeration process of 500 nm SiO_2 particles also undergoes three phases: plugging phase, channeling phase, and fluidization phase. At f = 30 Hz, Fig. 3b, the aeration processes of 500 nm SiO_2 particles is composed of two phases: plugging phase at low gas velocity and fluidization phase at relatively high gas velocity. It should be pointed out that no channels appear during aeration process because the sound wave energy breaks up the channels. At f = 40 Hz, the fluidized bed tends to fluidize with increasing superficial gas velocity.

As sound frequency approaches 50 and 60 Hz, Fig. 3d and e, 500 nm SiO_2 particles can be smoothly fluidized, in which u_{mf} reduces to 4.51 and 4.52 cm/s, respectively. It can be concluded that the bed has a good fluidization quality over a wide frequency range from 40 to 60 Hz.

As sound frequency raises 70 Hz, Fig. 3f, plugging, channeling, and gradual fluidization process occur continuously in the

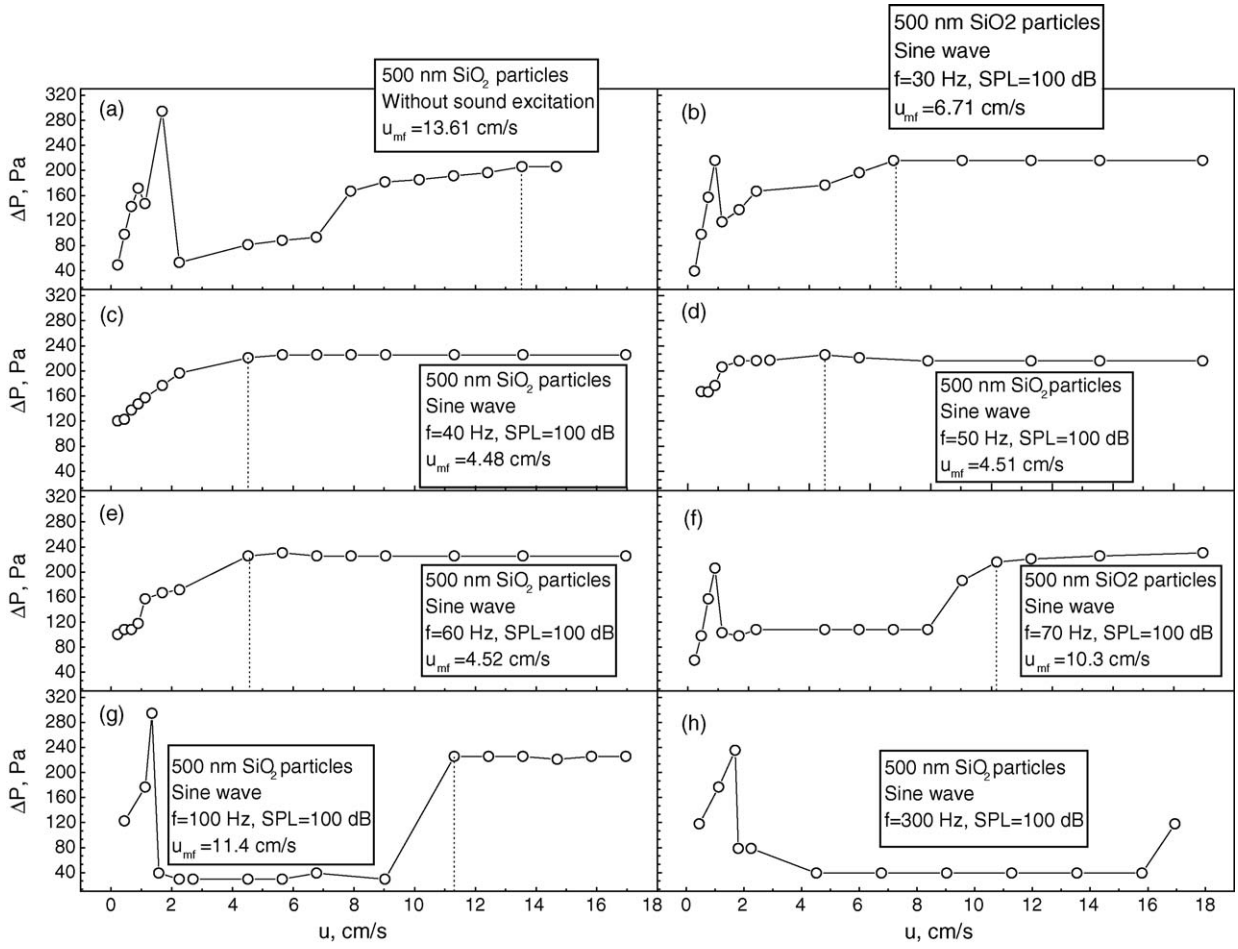

Fig. 3. Effect of sound frequency on the minimum fluidization velocity using 500 nm SiO_2 particles.

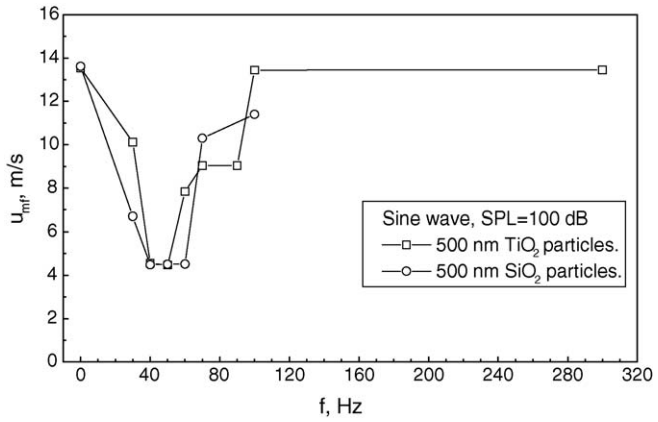

Fig. 4. Plot of minimum fluidization velocity vs. acoustic frequency for 500 nm TiO_2 particles and 500 SiO_2 particles.

bed with increasing gas velocity. In particular, channeling exists in the bed in a wide range from 1.30 to 7.91 cm/s, denoted that the relative high sound frequency fails to assist bed fluidization. At f = 100 Hz, Fig. 3g, plugging, channeling, and fluidization appears during an aeration process. By contrast, no homogeneous fluidization phenomena of SiO_2 particles can be observed at f = 300 Hz, Fig. 3h, as superficial gas velocity is greater than 17.06 cm/s.

3.3. Effect of sound frequency on minimum fluidization velocity

Fig. 4 exhibits the dependence of u_{mf} on the sound frequency for 500 nm TiO_2 particles and 500 nm SiO_2 particles at a given sound pressure level. For both type of the particles, u_{mf} initially decreases with frequency, and then increases dramatically after a critical sound frequency (F_{cr}). The critical frequency is defined as the frequency at which the minimum u_{mf} is obtained. In terms of the present investigation, the critical frequency ranges from 40 to 60 Hz for two types of nanometer particles. Xu et al. [13] employed a 100 mm i.d. Plexiglas bed using two type of micron meter particles (10 and 39 μm glass beads), indicating that the critical frequency is in the range 100–120 Hz. The difference in value of critical frequency may be attributed to natural frequency for gas–solid fluidized bed [14]. This calls for further effort.

3.4. Effect of sound pressure level on fluidization behaviors

Fig. 5 compares the fluidization curves under various sound pressure levels and at a given sound frequency. Fig. 5a reveals slugging occurring in the bed at u = 1.39 cm/s when sound pressure level approaches 100 dB. At SPL = 102.5 dB, the bed reaches homogeneous fluidization with fluidization behaviors similar to those of Geldart group A particles. As sound pressure level further increased to 103.4 dB, the bed completely fluidizes at u = 2.64 cm/s. A comparison of Fig. 5a–c demonstrates that the increasing pressure level lead to a significant reduction in minimum fluidization velocity. Similar conclusions can be drawn from Fig. 6a–c, where u_{mf} of 500 nm TiO_2 particles reduces from 6.74 to 5.76 cm/s, and then to 5.50 cm/s as sound pressure level varied from 100, 102.5, and to 103.4 dB. Obviously, sound waves with a high sound pressure level have relative greater energy which dissipates slugging and disrupts effectively almost nanoparticle agglomerates. In theory, the break-up of clusters into subclusters occurred at a contact points where the collision energy, sound energy, induced by the acoustic field exceed the internal van der Waals forces, i.e. cohesive force. In summary, one can be derived from Figs. 5 and 6 that good fluidization quality depends on appropriate sound pressure level and on sound frequency.

3.5. Effect of sound wave configurations on fluidization behaviors of ultrafine particles

To examine the influence of the wave forms on fluidization behaviors of ultrafine particles, two types of ultrafine particles

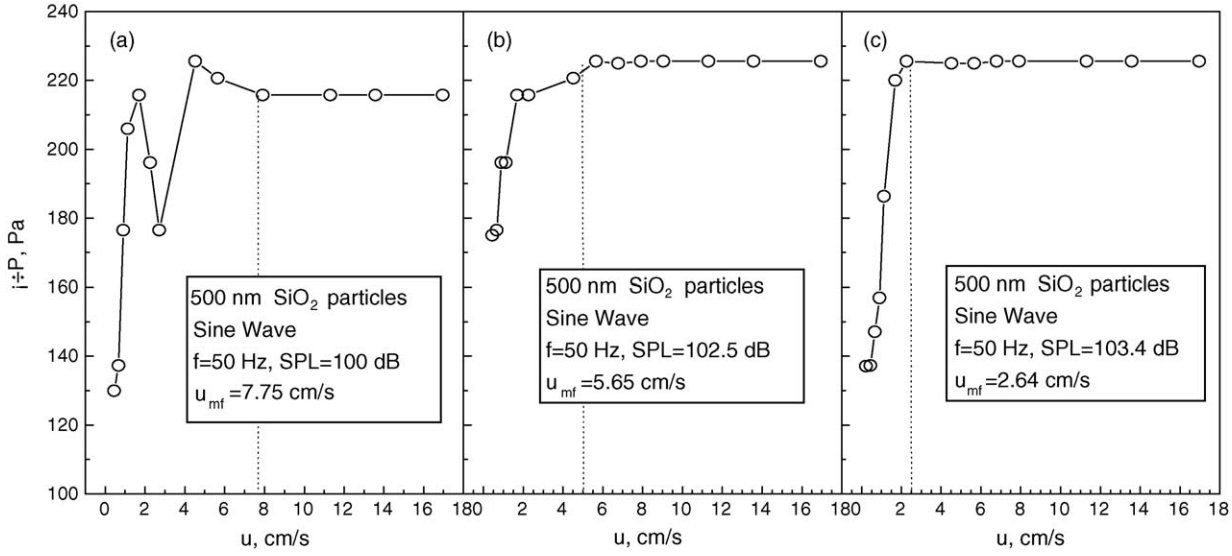

Fig. 5. Fluidization curves of cornstarch particles at a given sound frequency under various sound pressure levels.

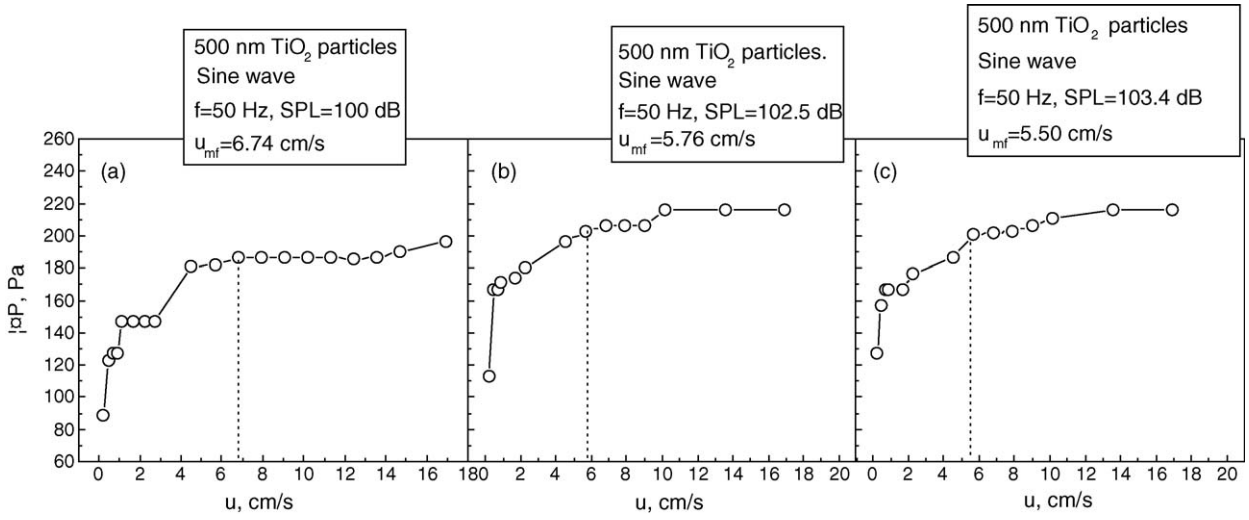

Fig. 6. Fluidization curves of 500 nm TiO_2 particles at a given sound frequency under various sound pressure levels.

were employed to the investigate fluidization process under various wave forms. Fig. 7 illustrates different wave forms, Sine wave in Fig. 7a, Triangle wave in Fig. 7b, Square wave in Fig. 7c, Rampup wave in Fig. 7d, sin(*x*)/*x* in Fig. 7e, tested at present research. As described in Fig. 8a, 10.69 μm cornstarch particles can arrive at a stable fluidization using sine wave and triangle wave. Under square wave excitation, the aeration process of cornstarch particles undergoes two phases: slugging and fluidization phase. Similarly, plugging and fluidization process phase also occur in the fluidization process using Rampup wave. However, plugging lasts much time until high minimum fluidization velocity. As sin(*x*)/*x* wave exerts on the bed, slugging phase, channeling phase, and fluidization process take place over an aeration process, like an aeration process of ultrafine particles without sound agitation. In this case, the bed can be smoothly fluidized at $u = 13.5$ cm/s.

It can be seen from Fig. 9 that 500 nm SiO_2 particles can be fully fluidized with the assistance of Sine wave and Triangle wave. On the other hand, three serial phases, plugging, channeling, and fluidization process appear in the bed using Square wave and Rampup wave. Note that no obvious fluidization comes up within the superficial gas velocity investigated. In conclusion, the fluidization quality of ultrafine particles can be improved greatly by using Sine wave and Triangle wave. In other word, the sound wave forms have a great influence on fluidization behaviors of ultrafine particles.

3.6. Sound pressure distribution of various sound wave forms in fluidized beds

The sound signal of Sine wave type can be written by

$$f(t) = \sin\left(\frac{2\pi}{20}t\right) = \sin\left(\frac{\pi}{10}t\right), \quad 0 < t < \infty \tag{2}$$

Sine wave is characterized by a continuous function with equal amplitudes.

The exponent expansion of sound signal of sin(*x*)/*x* type follows:

$$f(t) = \frac{\sin\left(\frac{2\pi}{20}t\right)}{t} = \frac{\sin\left(\frac{\pi}{10}t\right)}{t}, \quad 0 < t < \infty \tag{3}$$

The Fourier expansion of sound signal of triangle wave type can be given by

$$f(t) = \begin{cases} 10t, & t \in (0, 5) \\ -10t + 100, & t \in (5, 15) \\ 10t - 200, & t \in (15, 20) \end{cases} \tag{4}$$

$$f(t) = -\frac{400}{\pi^2}\left[\sin\frac{\pi t}{10} - \frac{1}{9}\sin\frac{3\pi t}{10} + \frac{1}{25}\sin\frac{5\pi t}{10} - \frac{1}{49}\sin\frac{7\pi t}{10} + \cdots + (-1)^{n+1}\frac{1}{(2n+1)^2}\sin\frac{2n+1}{10}\pi t\right], \quad 0 < t < +\infty \tag{5}$$

The triangle wave comprises a number of Sine waves, i.e. $\sin\left(\frac{\pi t}{10}\right)$, $\frac{1}{9}\sin\left(\frac{3\pi t}{10}\right)$, $\frac{1}{25}\sin\left(\frac{5\pi t}{10}\right)$, ..., $\frac{1}{(2n-1)^2}\sin\left(\frac{(2n-1)\pi t}{10}\right)$, with different frequencies, $\frac{1}{20}$, $\frac{3}{20}$, $\frac{5}{20}$, ..., $\frac{2n-1}{20}$. Nevertheless, the Triangle wave is a continuous function having same wave crest and wave trough through a period (20 ms).

The Fourier expansion of sound signal of square wave type can be expressed by

$$f(t) = \begin{cases} 50, & t \in (0, 10) \\ -50, & t \in (0, 20) \end{cases} \tag{6}$$

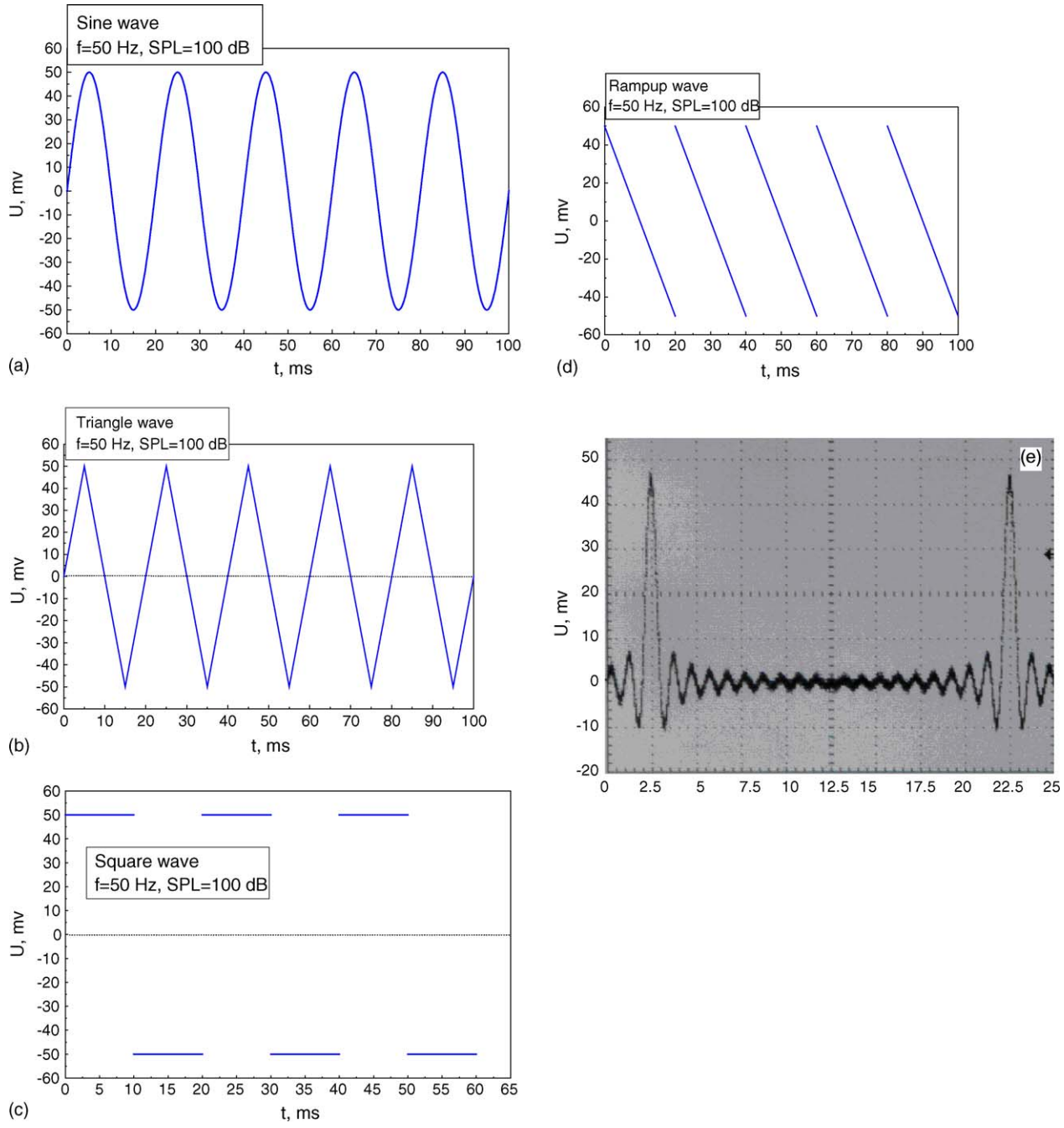

Fig. 7. Various wave types generated from a WY 1603 signal generator.

$$f(t) = -\frac{200}{\pi}\left(\sin\frac{\pi t}{10} + \frac{1}{3}\sin\frac{3\pi t}{10} + \frac{1}{5}\sin\frac{5\pi t}{10} + \cdots + \frac{1}{2n-1}\sin\frac{(2n-1)\pi t}{10}\right),$$
$$0 < t < +\infty, \quad t \neq 0, \pm 10, \pm 20, \ldots \tag{7}$$

The above equation consists of a series of sine waves, i.e. $\sin\left(\frac{\pi t}{10}\right)$, $\frac{1}{3}\sin\left(\frac{3\pi t}{10}\right)$, $\frac{1}{5}\sin\left(\frac{5\pi}{10}t\right), \ldots, \frac{1}{2n-1}\sin\left(\frac{(2n-1)\pi t}{10}\right)$, with various frequencies, $\frac{1}{20}, \frac{3}{20}, \frac{5}{20}, \ldots, \frac{2n-1}{20}$. The square wave is a complex wave composed of different Sine waves in nature, which is featured by a discontinuity function.

The Fourier expansion of sound signal of Rampup wave type can be presented by

$$f(t) = -5t + 50, \quad t \in (0, 20) \tag{8}$$

$$f(t) = -\frac{100}{\pi}\left(\sin\frac{\pi t}{10} - \frac{1}{2}\sin\frac{2\pi t}{10} + \frac{1}{3}\sin\frac{3\pi t}{10} - \frac{1}{4}\sin\frac{4\pi t}{10} + \cdots\right),$$
$$0 < t < +\infty, \quad t \neq \pm 10, \pm 20, \ldots \tag{9}$$

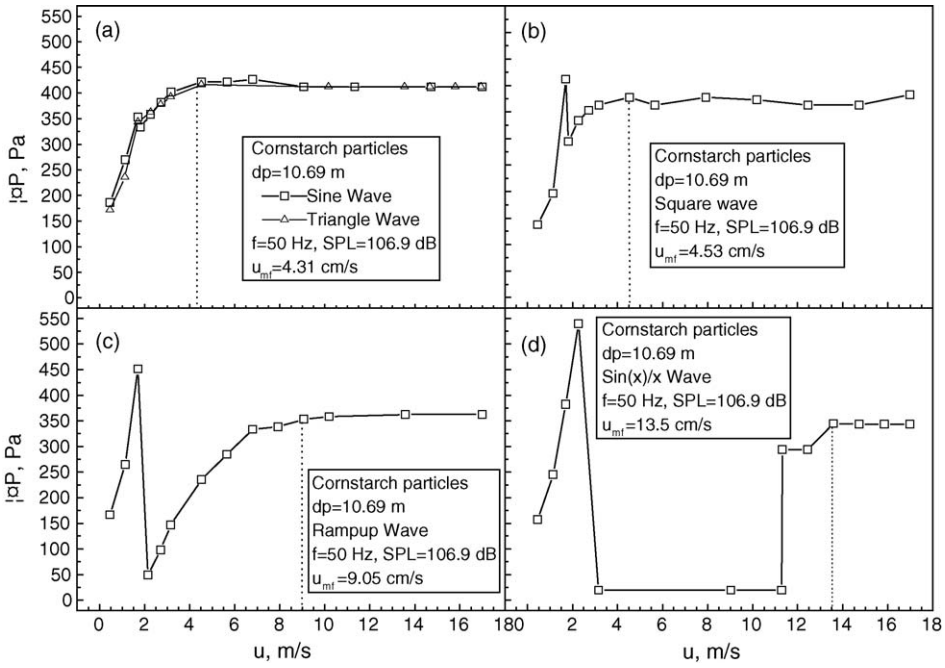

Fig. 8. Fluidization curves of cornstarch particles with various sound wave configurations.

The Rampup wave type is composed of a number of sine waves, i.e. $\sin\left(\frac{\pi t}{10}\right)$, $\frac{1}{2}\sin\left(\frac{2\pi t}{10}\right)$, $\frac{1}{3}\sin\left(\frac{3\pi}{10}t\right)$, ..., $\frac{1}{n}\sin\left(\frac{n\pi t}{10}\right)$, with various frequencies, $\frac{1}{20}$, $\frac{2}{20}$, $\frac{3}{20}$, ..., $\frac{n}{20}$. For each of Sine wave, wave trough and wave crest occur at different time over a period. Therefore, the describing parameters, such as period, frequency, and amplitude, of the overlap Sine wave are different from a single Sine wave. It is shown in Fig. 7d that Rampup wave tends to become a discontinuity wave.

In the fluidized bed, sound transmits into two single-phase media (gas and solid medium). Therefore, the media are responsible for change as the acoustic waves pass through each medium.

The incident wave pressure (P_i) and reflected wave pressure (P_r) can be expressed by

$$P_i = P_{ia}\, e^{j(\omega t - kx)} \tag{10}$$

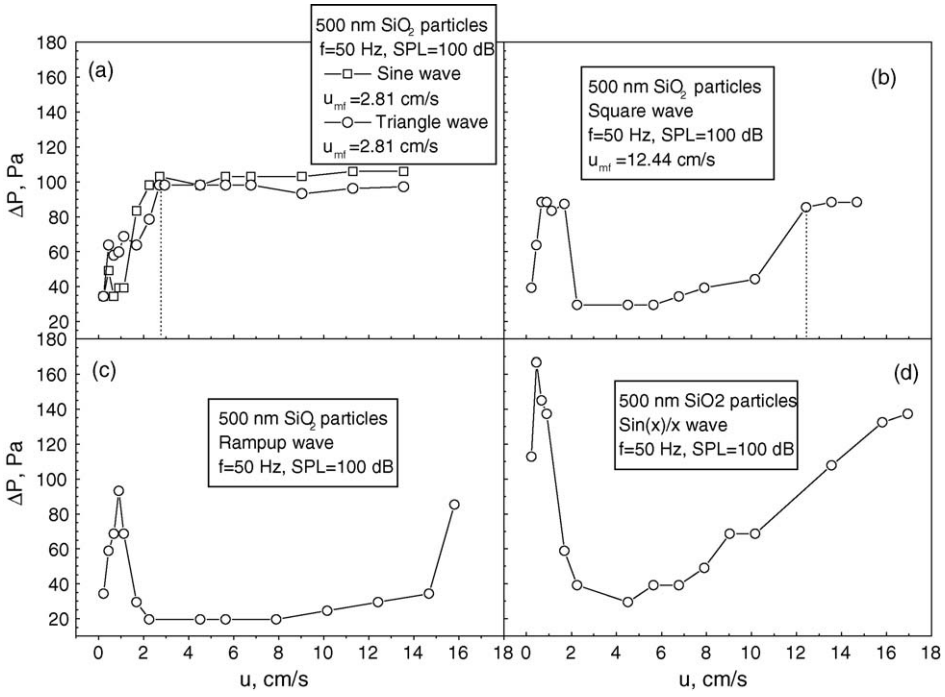

Fig. 9. Fluidization curves of various sound wave configurations (500 nm SiO_2 particles).

$$P_r = P_{ra}e^{j(\omega t+kx)} \tag{11}$$

According to the theory of Kinsler and Frey [15], the total pressure within the fluidized bed can be calculated as the sum of the incident and reflected waves

$$P(x,t) = P_i + P_r = P_{ia}[e^{-jkx} + |r_p|e^{j(kx+\sigma x)}]e^{j\omega t} = |P_a|e^{j(\omega t+\varphi)} \tag{12}$$

where reflected coefficient is depicted by $r_p = |r_p|e^{j\sigma\pi}$, $\sigma\pi$ the phase difference between incident wave and reflected wave, and k is the wave number, defined by

$$k = \frac{2\pi f}{c} \tag{13}$$

where f and c are sound frequency and sound speed, respectively.

On the interface of two media whose acoustic impedance has great difference in numerical value, reflected coefficient approximates

$$r_p \approx 1, \quad r_p \neq 1, \quad \delta \approx 1, \quad \sigma \neq 1 \tag{14}$$

The amplitude of total acoustic pressure is denoted by

$$|P_a| = p_{ia}\sqrt{2 + 2\cos 2k\left(x + \frac{\lambda\delta}{4}\right)} \tag{15}$$

where P_a and φ are amplitude of total acoustic pressure and fixed phase angle being independence of acoustic energy.

The acoustic energy density distribution in media is represented by

$$I = \frac{P_{ia}^2}{2\rho c} = \frac{P_{ia}^2}{2\rho c}\left[2 + 2\cos 2k\left(x + \frac{\lambda}{4}\right)\right]e^{j2(\omega t+\varphi)} \tag{16}$$

where ρ and c are media density and acoustic velocity in media, respectively.

Accordingly, various sound wave results in different acoustic energy density distribution in media. Sine wave and triangle wave are continuous function having same amplitude through a period, which causes an even energy density distribution in media at each period. Whereas, Square wave and Rampup wave are characterized by a discontinuity function, energy density fluctuates greatly between maximum value and minimum value. For $\sin(x)/x$, wave crest region lasts 1.5 ms, being account for 7.5% time over a period, 20 ms. There is an uneven energy density distribution in media over the operation time. The energy density distributions of various sound wave forms are consistent with the fluidization behaviors using different sound wave forms.

4. Conclusions

A series of experiments were performed in an acoustic fluidized bed to study the fluidization behaviors of various ultrafine particles using 500 nm TiO_2 particles, 500 nm SiO_2 particles and 10.69 μm cornstarch particles. The results shows that nanoparticles can arrive at stabilized fluidization at sound frequency in the range 40–70 Hz and sound pressure level greater than 100 dB. Such fluidization behaviors are similar to those of Geldart group A particles with no bubbles appearing and negligible elutriation. By contrast, at sound frequency exceeding 90 Hz, the aeration process encounters slugging and fluidization process accompanied by much elutriation.

At the same sound frequency, the fluidization quality of nanoparticles improves significantly with an increase in sound pressure level (100–103.4 dB). Furthermore, the minimum fluidization velocity tends to reduce as sound pressure level increases from 100 to 103.4 dB.

A series of investigations indicate that sound wave forms have a great influence on fluidization process of ultarfine particles. Both Sine wave and Triangle wave can enhance fluidization process of ultarfine particles. The energy density distribution of various sound wave forms is consistent with the fluidization behaviors using different sound wave forms.

Acknowledgments

The authors would like to acknowledge the Natural Science Foundation of Shandong Province (Contract No. Z2003B04), Project-sponsored by SRF for ROCS, SEM (Contract No. 2004527), and by Taishan Scholar Construction Project for financial support.

References

[1] C. Zhu, Q. Yu, R.N. Dave, R. Pfeffer, Gas fluidization characteristics of nanoparticle agglomerates, AIChE J. 51 (2005) 426–439.
[2] C.H. Nam, R. Pfeffer, R.N. Dave, S. Sundaresan, Aerated vibrofluidization of silica nanoparticles, AIChE J. 50 (2004) 1776–1785.
[3] Q. Yu, R.N. Dave, C. Zhu, J. Aquevedo, R. Pfeffer, Enhanced fluidization of nanoparticles in an oscillating magnetic field, AIChE J. 51 (2005) 1971–1979.
[4] Q. Guo, Y. Li, M.H. Wang, W. Shen, Fluidization behaviors for coating cohesive particles, Chem. Eng. Technol. 28 (2005) 752–756.
[5] R. Chirone, L. Massimilla, S. Russo, Bubble-free fluidization of a cohesive powder in an acoustic field, Chem. Eng. Sci. 48 (1993) 41–52.
[6] R. Chirone, L. Massimilla, Sound-assisted aeration of beds of cohesive solids, Chem. Eng. Sci. 49 (1994) 1185–1194.
[7] E.K. Levy, I. Shnitzer, T. Masaki, J. Salmento, Effect of an acoustic field on bubbling in a gas fluidized bed, Powder Technol. 90 (1997) 53–57.
[8] C.A. Herrera, E.K. Levy, J. Ochs, Characteristics of acoustic standing waves in fluidized beds, AIChE J. 48 (2002) 503–513.
[9] C.A. Herrera, E.K. Levy, Bubbling characteristics of soundassisted fluidized beds, Powder Technol. 119 (2001) 229–240.
[10] C. Zhu, G. Liu, R. Pfeffer, R. Dave, C. Nam, Sound assisted fluidization of nanoparticle agglomerates, Powder Technol. 141 (2004) 119–123.
[11] D. Wu, Z. Qian, D. Shao, Sound attenuation in a coarse granular medium, J. Sound. Vib. 162 (1993) 529–535.
[12] G. Ballou (Ed.), Handbook of Sound Engineers, 3rd ed., Focal Press, Woburn, 2002, MA01801-2041.
[13] Ch. Xu, Y. Cheng, J. Zhu, Fluidization of fine particles in a sound and identification of group C/A particles using acoustic waves, Powder Technol. 161 (2006) 227–234.
[14] R. Roy, J.F. Davison, V.G. Tuponogov, The velocity of sound in fluidized beds, Chem. Eng. Sci. 45 (1) (1990) 3233–3245.
[15] L.E. Kinsler, A.R. Frey, Fundamentals of Acoustics, Wiley, New York, 1962.